ARTICLE
PUBLISHED ONLINE: 28 APRIL 2014 | DOI: 10.1038/NCHEMBIO.1520
nature chemical biology

Plant perception of β-aminobutyric acid is mediated by an aspartyl-tRNA synthetase

Estrella Luna[1,2], Marieke van Hulten[3], Yuhua Zhang[2,8], Oliver Berkowitz[4,5], Ana López[1], Pierre Pétriacq[1], Matthew A Sellwood[6], Beining Chen[6], Mike Burrell[1], Allison van de Meene[2,8], Corné M J Pieterse[3], Victor Flors[7] & Jurriaan Ton[1–3]*

Specific chemicals can prime the plant immune system for augmented defense. β-aminobutyric acid (BABA) is a priming agent that provides broad-spectrum disease protection. However, BABA also suppresses plant growth when applied in high doses, which has hampered its application as a crop defense activator. Here we describe a mutant of *Arabidopsis thaliana* that is impaired in BABA-induced disease immunity (*ibi1*) but is hypersensitive to BABA-induced growth repression. *IBI1* encodes an aspartyl-tRNA synthetase. Enantiomer-specific binding of the *R* enantiomer of BABA to IBI1 primed the protein for non-canonical defense signaling in the cytoplasm after pathogen attack. This priming was associated with aspartic acid accumulation and tRNA-induced phosphorylation of translation initiation factor eIF2α. However, mutation of eIF2α-phosphorylating GCN2 kinase did not affect BABA-induced immunity but relieved BABA-induced growth repression. Hence, BABA-activated IBI1 controls plant immunity and growth via separate pathways. Our results open new opportunities to separate broad-spectrum disease resistance from the associated costs on plant growth.

Plants have evolved sophisticated strategies to defend themselves against pathogens. In addition to their preexisting defense barriers, plants can mobilize structural and chemical defense barriers that become active after pathogen attack. These inducible defenses are controlled by the plant's innate immune system, which provides protection against the majority of potentially harmful microorganisms. Regulation of plant immunity involves small-molecule hormones, such as salicylic acid (SA) and jasmonic acid[1]. To optimally adapt to hostile environments, plants can sensitize their basal immune system in response to specific alarm signals[2,3]. This so-called 'priming of defense' mediates a faster and stronger defense reaction to future pathogen attacks. A classic example comes from systemic acquired resistance, which is associated with priming of SA-inducible defenses in distal plant parts after localized pathogen attack[4,5]. Although priming of defense rarely provides complete protection against disease and is associated with fitness costs[6,7], it has the benefit that it boosts multi-genic basal resistance that relies on perception of multiple microbe- and damage-associated molecular patterns[8,9]. Accordingly, priming of defense offers broad-spectrum disease protection that is difficult to break by pathogens. Furthermore, priming typically provides long-lasting disease protection and can even be transmitted epigenetically to following generations[10,11]. Taken together, these characteristics make priming attractive for integration in sustainable crop protection[8,12].

The search for resistance-inducing chemicals in plants has yielded various compounds. These molecules are often (derivatives of) microbe-associated molecular patterns or plant-endogenous signaling molecules, such as SA, methyl-SA or azelaic acid[13]. When applied in relatively moderate quantities, these chemicals prime SA-inducible defenses. There are also plant-xenobiotic chemicals that can prime plant defense[2,14]. A well-known example is BABA. This nonprotein amino acid protects plants against an exceptionally broad spectrum of stresses, including crop diseases that are difficult to control by conventional strategies of disease management[15]. The broad-spectrum effectiveness of BABA-induced resistance (BABA-IR) is based on simultaneous priming of SA-dependent and SA-independent defense mechanisms[16,17]. The SA-dependent component of BABA-IR leads to augmented activation of SA-inducible defense genes and requires a functional NPR1 protein[16]. Previously, we identified three *Arabidopsis* mutations that differentially affect SA-dependent and SA-independent BABA-IR[17]. Recently, two additional *Arabidopsis* mutants in SA-dependent BABA-IR have been identified: the *lecrk-VI.2-1* mutant, which is affected in a receptor kinase gene[18], and the *ald1* mutant, which is impaired in pipecolic acid production[19]. SA-independent BABA-IR is associated with priming of pathogen-induced callose and requires intact biosynthesis and perception of the plant hormone abscisic acid (ABA)[17,20]. This priming of cell wall defense has also been linked to induced systemic resistance (ISR) after root colonization by *Pseudomonas fluorescens* WCS417r[21].

A major disadvantage of chemical priming agents is that overstimulation can lead to stress that affects plant growth[6]. These stress reactions have been attributed to the costs of direct induction of defense mechanisms, which often develops upon treatment with relatively high doses of the priming agent[7]. However, the BABA-induced stress response seems to be more specific and has been related to perturbations in amino acid homeostasis[22]. This undesirable side effect of BABA has hindered exploitation of the agent as a crop defense activator, despite its extraordinary wide range of effectiveness[15].

In this study, we identify the *IMPAIRED IN BABA-INDUCED IMMUNITY 1 (IBI1)* gene as a new master regulator of BABA-IR. *IBI1* encodes an aspartyl-tRNA synthetase (AspRS). We provide evidence that the active *R* enantiomer of BABA binds the IBI1 protein

[1]Department of Animal and Plant Sciences, The University of Sheffield, Sheffield, UK. [2]Rothamsted Research, Harpenden, UK. [3]Department of Biology, Utrecht University, Utrecht, The Netherlands. [4]Australian Research Council Centre of Excellence in Plant Energy Biology, University of Western Australia, Perth, Australia. [5]School of Plant Biology, University of Western Australia, Perth, Australia. [6]Department of Chemistry, University of Sheffield, Sheffield, UK. [7]Departmento de Ciencias Agrarias y del Medio Ambiente, University of Jaume I, Castellon, Spain. [8]Present addresses: Research and Development Center, Firmenich Aromatics (China) Co. Ltd., Shanghai, China (Y.Z.); School of Botany, The University of Melbourne, Victoria, Australia (A.v.d.M.). *e-mail: j.ton@sheffield.ac.uk

and interferes with canonical AspRS activity. This interaction primes IBI1 for noncanonical defense activity against pathogen attack and simultaneously activates a separate stress pathway that results in plant growth repression. Our study shows that the benefits of broad-spectrum disease resistance can be separated from the associated costs, providing new opportunities to improve chemical induction of broad-spectrum disease resistance without affecting crop growth.

RESULTS

The *ibi1* mutant

BABA-treated *Arabidopsis* develops full immunity against the biotrophic downy mildew pathogen *Hyaloperonospora arabidopsidis*, which acts independently from the SA- and NPR1-dependent pathway[16,17]. To search for new signaling components in this SA-independent immune response, we screened an ethyl methanesulfonate (EMS)-mutagenized M2 population of SA nonaccumulating Col-0 NahG[23] for *ibi* mutants against *H. arabidopsidis*. Evaluation of 34,200 plants from 57 M2 pools yielded two putative *ibi* mutants from different pools, whose phenotype could be confirmed in the M3 generation. No complementation of the *ibi* phenotype was observed in F2 progeny from a cross between both mutants ($n > 50$), whereas F2 progeny from a backcross between NahG *ibi1-1* with NahG displayed monogenic 1:3 segregation of the mutant phenotype ($\chi^2 = 0.144$; $P = 0.704$). These results indicate that both mutations, termed *ibi1-1* and *ibi1-2*, are recessive and allelic.

Microscopic analysis of Trypan blue–stained leaves confirmed that leaves of NahG *ibi1-1*, unlike those of NahG, failed to arrest *H. arabidopsidis* colonization after treatment of the roots with 150 µM BABA (**Fig. 1a** and **Supplementary Results**, **Supplementary Fig. 1a**). Epifluorescence microscopy of aniline blue– and calcofluor-stained leaves revealed that BABA-treated NahG *ibi1-1* did not deposit augmented levels of pathogen-arresting callose 2 d post inoculation (dpi) with *H. arabidopsidis* conidiospores (**Supplementary Fig. 1b**). Hence, *IBI1* controls SA-independent priming of cell wall defense. The NahG *ibi1-1* mutant was also impaired in SA-independent BABA-IR against the necrotrophic fungus *Plectosphaerella cucumerina* (**Supplementary Fig. 1c**), demonstrating that *IBI1* controls BABA-IR against biotrophic and necrotrophic pathogens. BABA-induced priming of cell wall defense against necrotrophic fungi requires intact responsiveness to the plant hormone ABA[20,24]. However, both NahG and NahG *ibi1-1* developed equal levels of ABA-induced resistance against *P. cucumerina* (**Supplementary Fig. 1c**). It can thus be concluded that the *ibi1-1* mutation does not affect ABA-induced defense, which suggests that IBI1 acts upstream of ABA in the BABA-IR pathway.

IBI1 encodes a class II AspRS

Mapping of the *ibi1-1* mutation was performed in a F2 population from a cross between NahG *ibi1-1* and the Landsberg *erecta* (L*er*) *rpp5* mutant[25], which is susceptible to *H. arabidopsidis* WACO9. Apart from the *ibi1-1* allele and the *NahG* transgene, other genetic determinants from Col-0 and L*er* parents segregated in this mapping population, causing a gradient of susceptibility phenotypes to *H. arabidopsidis*. Approximately 14,000 F2 plants were screened for loss of BABA-IR against *H. arabidopsidis*, of which only 1,204 individuals displayed sporulation by 7 dpi. Using sequence length polymorphism markers and (derived) cleaved amplified polymorphic sequence markers[26], the *ibi1-1* mutation was mapped to a region on the lower arm of chromosome IV, encompassing 64 candidate genes. Sanger sequencing of cDNA-derived PCR products identified a stop mutation in the first translated exon of *At4g31180* (**Fig. 1b**), which encodes a class II AspRS. Subsequent sequencing of *At4g31180* from NahG *ibi1-2* revealed a different stop mutation in the same exon of the gene (**Fig. 1b**).

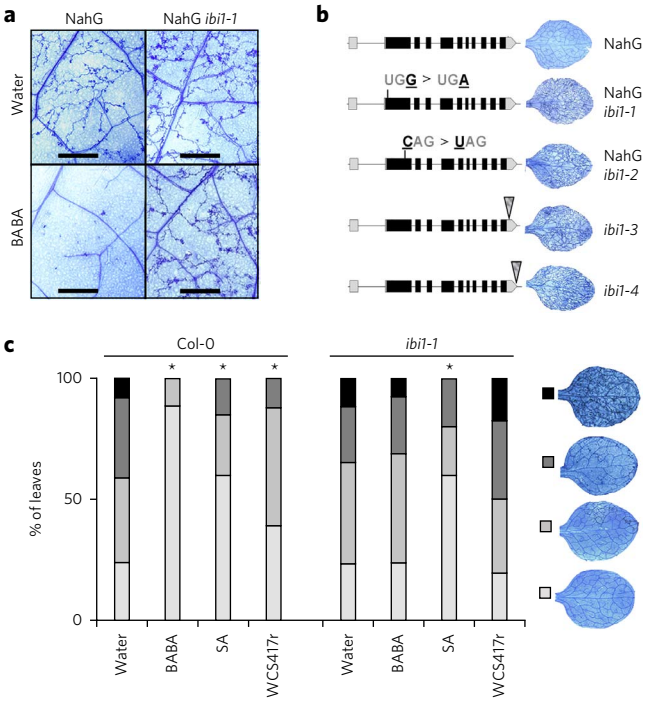

Figure 1 | Identification and characterization of the *Arabidopsis ibi1* mutant. (**a**) The NahG *ibi1-1* mutant does not express induced resistance against *H. arabidopsidis* WACO9 after root treatment with BABA (150 µM). Photographs of Trypan blue–stained leaves show representative differences in pathogen colonization at 7 d after inoculation. Scale bars, 1 mm. (**b**) Genomic structure of *IBI1* (*At4g31180*) and locations of *ibi1-1* (EMS mutation), *ibi1-2* (EMS mutation), *ibi1-3* (T-DNA insertion mutation)) and *ibi1-4* (T-DNA insertion mutation) mutations (underlined). Insets illustrate representative levels of *H. arabidopsidis* colonization in leaves of BABA-treated plants. (**c**) Levels of induced resistance against *H. arabidopsidis* WACO9 in Col-0 and *ibi1-1* after root treatment with BABA (150 µM), *P. fluorescens* WCS417r (5×10^7 cells per g soil) or shoot treatment with SA (0.5 mM). Insets show different classes of pathogen colonization; asterisks indicate statistically significant differences in class distribution relative to water-treated plants (Fisher's exact test, $P < 0.01$, $n = 50$–100).

IBI1 controls priming of multiple defense responses

To confirm that mutations in *At4g31180* are responsible for the *ibi1* phenotype, we evaluated phenotypes of two additional transfer DNA (T-DNA) insertion mutants, *ibi1-3* and *ibi1-4* (**Fig. 1b**). Despite the fact that these mutations are in the genetic background of the SA-producing Col-0 accession, both mutants failed to express BABA-IR against *H. arabidopsidis* (**Supplementary Fig. 2a**). Similarly, the *ibi1-1* mutation crossed into the Col-0 background blocked BABA-IR against *H. arabidopsidis* (**Fig. 1c** and **Supplementary Fig. 2a**). The absence of BABA-IR in *ibi1-1* was associated with the lack of augmented cell wall defense (**Supplementary Fig. 2b**). Hence, mutations in *At4g31180* cause the *ibi1* phenotype and can block BABA-IR in the background of SA-producing Col-0. Considering that SA-dependent resistance is highly effective against *H. arabidopsidis*[27], this suggests that *IBI1* controls both SA-dependent and SA-independent BABA-IR. However, application of 0.5 mM SA to shoots of *ibi1-1* induced wild-type levels of resistance against *H. arabidopsidis* (**Fig. 1c**), demonstrating that *IBI1* does not regulate SA-induced defense directly. As SA-dependent BABA-IR is based on priming of SA-dependent genes, rather than direct induction of SA-dependent defense[16,17,21], we tested BABA-induced priming of SA-induced *PR1* gene expression. BABA-treated *ibi1-1* failed

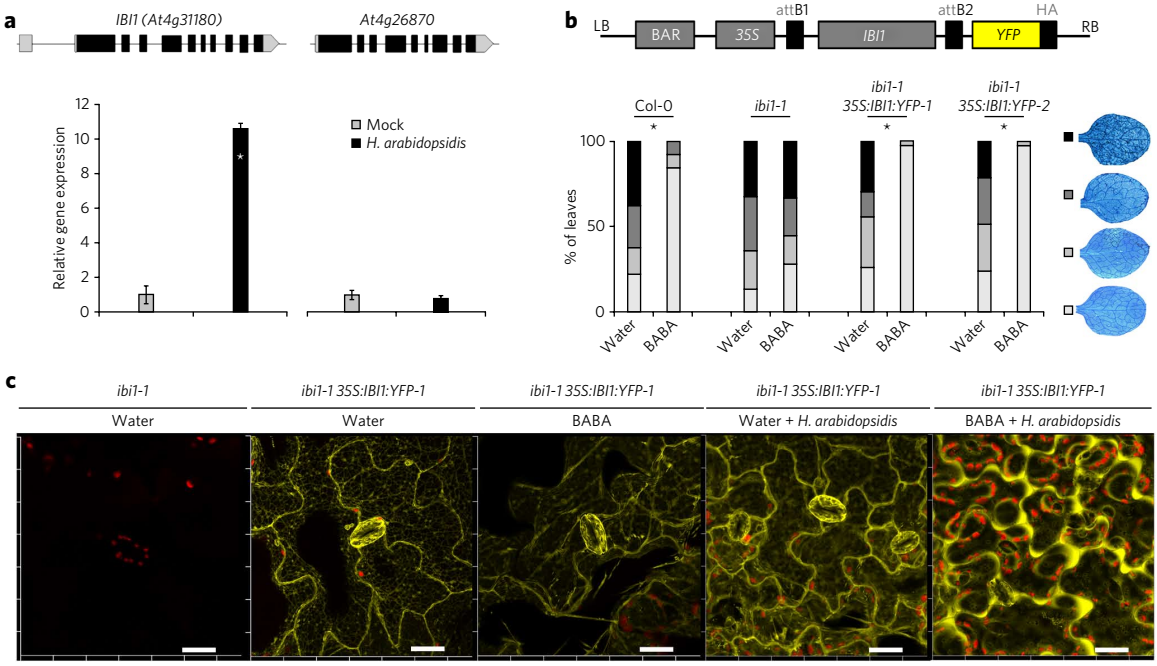

Figure 2 | Characterization of the defense function of *IBI1*. (**a**) Transcript accumulation of *IBI1* and its close homolog *At4g26870* in Col-0 at 5 dpi with *H. arabidopsidis* WACO9. Data represent average gene expression values (±s.e.m.) relative to mock-inoculated plants. Asterisk indicates a statistically significant difference between treatments (Student's *t*-test, $P < 0.05$, $n = 3$). (**b**) Transformation of *ibi1-1* with *35S:IBI1:YFP* restores induced resistance against *H. arabidopsidis* WACO9 after root treatment with BABA (150 μM). Insets show different classes of pathogen colonization; asterisks indicate statistically significant differences in class distribution relative to water-treated plants (Fisher's exact test, $P < 0.01$, $n = 50$–100). LB, left border; BAR, bialaphos resistant gene; attB/attB2, gateway recombination sequences; HA, human influenza hemagglutinin tag; RB, right border. (**c**) Confocal laser-scanning microscopy analysis of subcellular IBI1:YFP in *35S:IBI1:YFP-1* plants at 2 d after root treatment with water or BABA (150 μM) and 5 d after subsequent *H. arabidopsidis* WACO9 inoculation. Yellow indicates fluorescence by IBI1:YFP; red indicates chlorophyll fluorescence from chloroplasts. Left panel shows lack of YFP fluorescence in untransformed *ibi1-1* plants. Scale bars, 20 μm.

to show augmented *PR1* gene induction after SA application to the leaves, whereas BABA-treated Col-0 showed augmented *PR1* induction compared to water-treated plants 4 h after SA application (**Supplementary Fig. 2c**). BABA-treated *ibi1-1* also failed to display augmented *PR1* gene induction after inoculation with *H. arabidopsidis* (**Supplementary Fig. 2d**). Thus, the *ibi1-1* mutation blocks BABA-induced priming of both SA-dependent and SA-independent defense.

ISR against *H. arabidopsidis* after root colonization by *P. fluorescens* WCS417r is associated with SA-independent priming of cell wall defense and shares signal transduction components with BABA-IR[21]. To examine possible involvement of IBI1 in ISR, wild-type and *ibi1-1* plants were grown on *P. fluorescens* WCS417r-containing soil and evaluated for resistance against *H. arabidopsidis*. As is shown in **Figure 1c**, *P. fluorescens* WCS417r elicited ISR in the wild type but not in *ibi1-1*. Hence, *IBI1* not only is critical for BABA-IR but also controls rhizobacteria-mediated ISR.

IBI1 responds to pathogen attack

The *IBI1* gene encodes an AspRS that catalyzes biosynthesis of aspartyl-tRNA through esterification of L-aspartic acid (L-Asp) to cognate $tRNAs^{Asp}$ (ref. 28). The *Arabidopsis* genome contains two close AspRS gene homologs, *IBI1* and *At4g26870*. The corresponding proteins show 74% identity and 84% similarity in amino acid sequence (**Supplementary Fig. 3a**). Quantitative real-time PCR (RT-qPCR) analysis revealed that *At4g26870* is expressed to a level only 6% of that of IBI1 (**Supplementary Fig. 3b**), which is in agreement with publicly available transcriptome data. A homozygous T-DNA mutant in *At4g26870* (polymorphism SALK_030485) was fully capable of expressing BABA-IR (**Supplementary Fig. 3c**), demonstrating that the AspRS encoded by *At4g26870* has no alternative defense activity. Notably, *IBI1* gene transcription was not influenced by BABA (**Supplementary Fig. 4**). This indicates that BABA-IR by IBI is regulated by post-transcriptional processes. In contrast, *IBI1*, unlike *At4g26870*, showed increased transcription in response to *H. arabidopsidis*, (**Fig. 2a**), suggesting defense regulatory activity independently of BABA.

To study the subcellular localization of IBI1, we created transgenic lines in the *ibi1-1* background, expressing recombinant *IBI1:YFP* under constitutive control by the 35S cauliflower mosaic virus promoter. Two independent lines displayed a 31- and 32-fold increase in *IBI1* transcript levels compared to uninfected Col-0 plants (**Supplementary Fig. 5a**). This level of *IBI1* expression was sufficient to fully restore BABA-IR against *H. arabidopsidis* (**Fig. 2b**), demonstrating cellular functionality of recombinant IBI1-YFP protein. Both overexpression lines also showed increased basal resistance to *H. arabidopsidis*, which was particularly pronounced at 5 dpi and associated with augmented expression of pathogen-induced cell wall defense and SA-induced *PR1* transcription (**Supplementary Fig. 5c,d**). Considering that *IBI1* transcription was enhanced during *H. arabidopsidis* infection (**Fig. 2a**), these results demonstrate that elevated *IBI1* transcription contributes to basal resistance in the absence of BABA. Confocal laser scanning microscopy revealed that IBI1-YFP is predominantly localized at the endoplasmic reticulum (ER) and cytoplasmic strands surrounding the ER (**Fig. 2c**). This subcellular localization was confirmed by colocalization analysis of IBI1-YPF with CFP- and GFP-tagged ER markers[29] in double transgenic F1 progenies from a cross between *ibi1-1 35S:IBI1:YFP-1* and ER-marker lines (**Supplementary Fig. 6**). BABA treatment alone did not alter the subcellular localization of IBI1-YFP (**Fig. 2c**). However, inoculation of unprimed plants with *H. arabidopsidis* caused a minor shift of IBI1-YFP to the cytoplasmic

periphery of the cell (**Fig. 2c**). Notably, this subcellular response to *H. arabidopsidis* was markedly increased in BABA-treated plants, where IBI1-YFP was almost exclusively translocated to the peripheral cytoplasm (**Fig. 2c** and **Supplementary Fig. 7**). As plant aminoacyl-tRNA proteins are targeted to either plastids, mitochondria or cytoplasm[30], we conclude that BABA primes pathogen-inducible translocation of IBI1 within the cytoplasmic domain from the cytoplasmic strands surrounding the ER to the cytoplasmic periphery of the cell.

BABA binds to IBI1 in an enantiomer-specific manner

The chemical structure of L-Asp is markedly similar to that of the *R* enantiomer of BABA ((*R*)-BABA; **Fig. 3a**). Previous studies have shown that (*R*)-BABA is the active enantiomer for induced resistance in tobacco, cauliflower and lettuce[31–33]. The similarity between L-Asp and (*R*)-BABA prompted us to investigate whether BABA-IR in *Arabidopsis* is also determined by its *R* enantiomer. Of the two enantiomers, only (*R*)-BABA induced resistance against *H. arabidopsidis* (**Fig. 3a**). A similar enantiomer-specific effect was found for BABA-IR in tomato against *Botrytis cinerea* (**Supplementary Fig. 8**). Hence, BABA is perceived in a mechanistically similar manner across taxonomically unrelated plant species. Application of 150 µM BABA together with L-Asp to *Arabidopsis* mildly reduced BABA-IR to *H. arabidopsidis* (**Supplementary Fig. 9a**), suggesting competition between BABA and L-Asp. Treatment with 150 µM L-Asp alone failed to induce disease resistance (**Fig. 3a**), although a tenfold higher concentration of L-Asp (1.5 mM) resulted in a relatively weak increase in resistance (**Supplementary Fig. 9b**). However, the latter resistance response was also present in *ibi1-1* plants, suggesting an IBI1-independent stress response to application of high levels of L-Asp.

To explore the possibility that (*R*)-BABA binds to the L-Asp–interacting site of IBI1, we modeled protein-amino acid interactions using information from crystallized AspRS proteins of *Pichia pastoris* and *Pyrococcus kodakaraensis*. Previous site-directed mutagenesis studies with *P. pastoris* have revealed the L-Asp–, ATP- and tRNA-interacting protein domains of AspRS[34], which are conserved between *Arabidopsis* IBI1, *P. pastoris* AspRS and *P. kodakaraensis* AspRS (**Supplementary Fig. 10**). Owing to the availability of a crystallized co-structure of *P. kodakaraensis* AspRS and L-Asp at relatively high resolution (1.9 Å)[35], our computational docking models of BABA to the L-Asp–binding domain were based on *P. kodakaraensis* AspRS (Protein Data Bank (PDB) code 3NEL). Binding of L-Asp to AspRS produced the lowest energy complex in comparison to (*R*)-BABA and (*S*)-BABA (**Supplementary Fig. 11**). The difference in binding energy between L-Asp and (*R*)-BABA was 7.25 kcal mol^{-1}, which can be attributed to the loss of two weak hydrogen-bonding interactions between the side chain carboxylic acid group of L-Asp and the AspRS binding residues Ser487 and Asp331. However, the stronger backbone interactions between Asp348 and Ser307 (via a bridging water molecule) were retained for (*R*)-BABA. Furthermore, Van der Waals and hydrophobic interactions between the proximal methyl group of BABA and the binding site would partially compensate for the loss of the carboxylic acid group in comparison of L-Asp. The energy difference between L-Asp and (*S*)-BABA binding was 11.74 kcal mol^{-1}. This relatively weak binding affinity between (*S*)-BABA and IBI1 is due to the loss of another hydrogen bond between the bridging water molecule and the amino group of (*S*)-BABA. Consequently, (*S*)-BABA oriented in a nonfavorable direction for hydrogen bonding and structural fitting into the protein's binding cavity (**Supplementary Fig. 11**). Our models suggest that (*R*)-BABA binds with a greater affinity than (*S*)-BABA to the aspartic acid–binding pocket of AspRS.

To experimentally confirm enantiomer-specific binding of BABA to IBI1, wild-type (Col-0) and functionally complemented *ibi1-1 35S:IBI1:YFP-1* were treated with water, (*R*)-BABA or (*S*)-BABA.

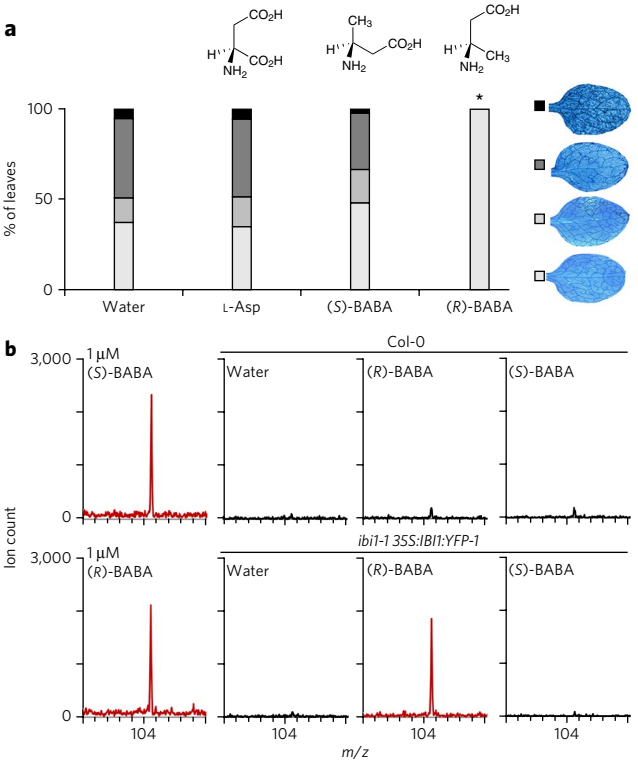

Figure 3 | Enantiomer-specific activity of BABA to IBI1. (**a**) Levels of induced resistance against *H. arabidopsidis* WACO9 in *Arabidopsis* (Col-0) after root treatment with L-Asp (150 µM), (*R*)-BABA (150 µM) or (*S*)-BABA (150 µM). Insets show different classes of pathogen colonization; asterisk indicates a statistically significant difference in class distribution relative to water-treated plants (Fisher's exact test, $P < 0.01$, $n = 50$–100). (**b**) MS analysis of BABA from immunoprecipitated IBI1:YFP of *ibi1-1 35S:IBI1:YFP-1* or untransformed Col-0 (negative control), using MALDI-qTOF ([M+H]; $m/z = 104{,}025$). Left panels show standards ((*R*)-BABA and (*S*)-BABA; 1 µM). IP was performed with protein extracts from leaves after two successive root treatments with water (control), (*R*)-BABA (1.2 mM) or (*S*)-BABA (1.2 mM). MALDI-qTOF analysis of IP extracts from *ibi1-1 35S:IBI1:YFP-1* plants after (*R*)-BABA or (*S*)-BABA applications was repeated twice from material of independent experiments, yielding similar results.

Subsequently, IBI1:YFP in plant protein extracts was immunoprecipitated and analyzed by MS for the presence of BABA. Using both MALDI-qTOF and ESI-quadrupole TOF (qTOF) analysis, we detected substantial quantities of BABA in the immunoprecipitated IBI1:YFP fraction from (*R*)-BABA–treated *ibi1-1 35S:IBI1:YFP-1* plants (**Fig. 3b** and **Supplementary Fig. 12**). Conversely, we detected only traces of BABA in the immunoprecipitated IBI1:YFP fraction of (*S*)-BABA–treated *ibi1-1 35S:IBI1:YFP-1* plants, which were comparable to levels from (*R*)-BABA–treated Col-0 lacking the YFP epitope for immunoprecipitation (IP; **Fig. 3b** and **Supplementary Fig. 12**). Thus, BABA binds in an enantiomer-specific manner to IBI1 *in planta*.

BABA blocks canonical AspRS activity of IBI1

To explore the impact of BABA binding to IBI1, we examined the effects of BABA on AspRS activity. As IBI1:YFP functionally restores BABA-IR in the *ibi1-1* mutant (**Fig. 2b**), we used immunoprecipitated IBI1:YFP to assay *in vitro* AspRS activity. However, despite various experimental variations of the assay (**Supplementary Table 1**)[36–39], we failed to detect *in vitro* ATP-pyrophosphate exchange activity by IBI1:YFP. Subsequent experiments revealed that IBI1:YFP loses enantiomer-specific binding activity to BABA

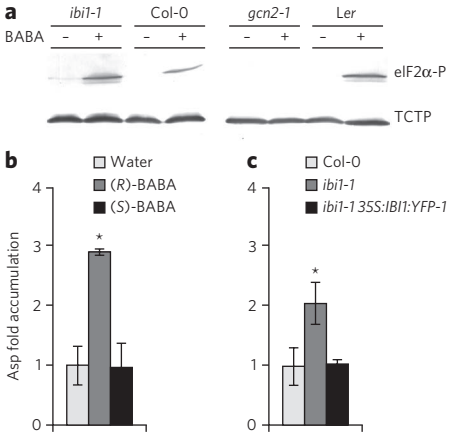

Figure 4 | BABA interferes with canonical AspRS activity. (**a**) Western blot analysis of eIF2α phosphorylation (Ser51) and TCTP (loading control) in *ibi1-1*, Col-0, *gcn2-1* and Ler 2 d after spraying the leaves with BABA (250 μM). (**b**) MALDI-qTOF quantification of aspartic acid levels in leaves of Col-0 2 d after root treatment with water, (*R*)-BABA (250 μM) or (*S*)-BABA (250 μM). (**c**) MALDI-qTOF quantification of aspartic acid levels in leaves of Col-0, *ibi1-1* and *ibi1-1 35S:IBI1:YFP-1*. Data in **b** and **c** represent average fold change values in comparison to basal aspartic acid levels in water-treated Col-0. Asterisks indicate statistically significant differences in comparison to water-treated Col-0 (Student's *t*-test, $P < 0.05$, $n = 3$–5).

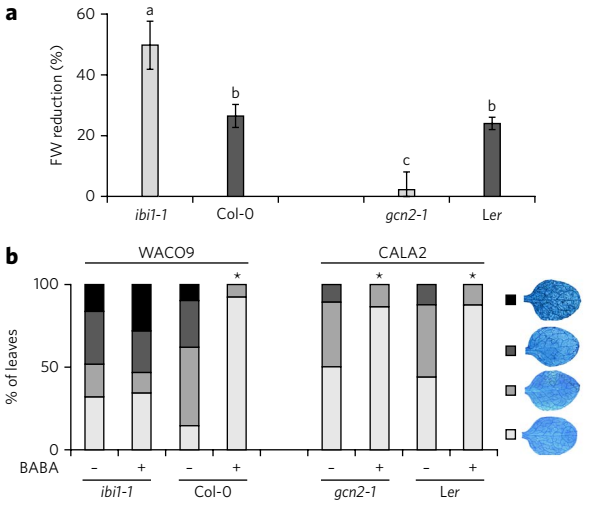

Figure 5 | Genetic separation of BABA-IR and growth repression. (**a**) BABA-induced growth suppression in *ibi1-1*, Col-0, *gcn2-1* and *Ler* at 1 week after root treatment with BABA (400 μM). Shown are mean percentages (±s.e.m.) of fresh weight (FW) reduction in BABA-treated plants relative to water-treated plants. Different letters indicate statistically significant differences between genotypes (Fisher's least significant differences test; $P < 0.05$). (**b**) Levels of induced resistance against *H. arabidopsidis* WACO9 (Col-0 and *ibi1-1*) and *H. arabidopsidis* CALA2 (*Ler* and *gcn2-1*) after root treatment with BABA (150 μM). Insets show different classes of pathogen colonization; asterisks indicate statistically significant differences in class distribution relative to water-treated plants (Fisher's exact test, $P < 0.01$, $n = 50$–100).

during protein purification (**Supplementary Fig. 13**), indicating that IBI1 functionality is affected when the protein is extracted from its cellular context, probably owing to the lack of interacting co-factors under *in vitro* conditions. We therefore continued with an alternative *in planta* approach to study the impact of BABA on AspRS activity.

In both yeast and *Arabidopsis*, the protein kinase GCN2 phosphorylates eukaryotic translation initiation factor eIF2α in response to hyperaccumulation of uncharged tRNA[40,41]. Accordingly, we used eIF2α phosphorylation to test whether BABA inhibits AspRS activity, thereby increasing accumulation of uncharged tRNA substrate. Western blot analysis confirmed that BABA induces eIF2α phosphorylation in Col-0, *ibi1-1* and L*er* plants but not in the *gcn2-1* mutant[42] (**Fig. 4a** and **Supplementary Fig. 14**). Hence, BABA activates GCN2, presumably by hindering *in planta* aminoacylation activity of tRNA synthetases. Notably, *ibi1-1* plants displayed faint eIF2α phosphorylation in the absence of BABA and increased eIF2α phosphorylation after BABA treatment (**Fig. 4a** and **Supplementary Fig. 14**). This suggests that AspRS activity from the relatively low-expression *At4g26870* gene is also sensitive to perturbation by BABA. It is plausible that the limited AspRS activity of the *ibi1-1* mutant increases its sensitivity to BABA-induced AspRS inhibition, leading to augmented accumulation of uncharged tRNA and GCN2 activity.

To confirm the impact of BABA on AspRS activity, we used MALDI-qTOF analysis to measure aspartic acid levels in leaf extracts of wild-type plants following root treatment with either (*R*)-BABA or (*S*)-BABA. Treatment with active (*R*)-BABA increased *in planta* Asp levels by threefold, whereas the inactive *S* enantiomer had no effect (**Fig. 4b**). Because aspartic acid is a substrate of AspRS, these results strengthen our conclusion that BABA obstructs canonical AspRS activity.

Finally, we compared aspartic acid levels in leaf tissues between wild-type, *ibi1-1* and *ibi1-1 35S:IBI1:YFP-1* plants to verify *in planta* AspRS activity by IBI1 (**Fig. 4c**). As can be expected for a genotype affected in AspRS activity, *ibi1-1* displayed enhanced aspartic acid accumulation, which reverted to wild-type levels in *ibi1-135S:IBI1:YFP-1* plants. Together with the observation that *ibi1-1* displays augmented activity of tRNA-induced GCN2 (**Fig. 4a**), these results confirm that *IBI1* functions as an AspRS enzyme.

IBI1 controls resistance and growth via separate pathways

Apart from inducing broad-spectrum resistance, BABA is also known to suppress plant growth[6,22]. To test the role of IBI1 in this stress response, growth rates of wild-type and *ibi1-1* seeds were assayed on BABA-containing agar plates (400 μM). To our surprise, *ibi1-1* seedlings on BABA-containing agar stopped growing immediately after seed germination or failed to germinate altogether, whereas wild-type seeds managed to germinate and grow under these conditions (**Supplementary Fig. 15a**). This hypersensitivity to BABA was only apparent upon treatment with the *R* enantiomer of BABA and functions independently from SA, as NahG *ibi1-1* displayed similar stress sensitivity to *ibi1-1* (**Supplementary Fig. 15a**,**b**). The difference in BABA-induced stress between wild-type and *ibi1-1* plants was also apparent at later developmental stages: 1 week after BABA application to roots of 3-week-old plants, *ibi1-1* had 50% lower shoot fresh weight values compared to that in control-treated *ibi1-1*, whereas the BABA-treated wild type only exhibited a 26% reduction in shoot fresh weight (**Fig. 5a**). In a separate experiment, the SALK_030485 mutant in the *IBI1* homolog *At4g26870* had wild-type levels of BABA-induced growth repression (**Supplementary Fig. 16a**). Considering that *At4g26870* is expressed to only 6% of *IBI1* (**Supplementary Fig. 3b**), we conclude that the relatively small reduction in total AspRS of the SALK_030485 mutant is not sufficient to cause detectable levels of hypersensitivity to BABA-induced stress. By contrast, overexpression of IBI1 in *ibi1-1 35S:IBI1:YFP-1* provided enhanced tolerance to BABA-induced growth repression (**Supplementary Fig. 16b**), as can be expected from a genotype with increased BABA-binding capacity.

BABA-induced plant stress is associated with perturbations in amino acid homeostasis in *Arabidopsis*[22]. Considering that eIF2α phosphorylation by GCN2 affects amino acid metabolism in yeast,

we investigated the possibility that GCN2 controls BABA-induced growth repression. Comparison of the *gcn2-1* mutant to its corresponding wild-type (L*er*) revealed that the *gcn2-1* mutation is more tolerant to BABA-induced growth repression (**Fig. 5a**), confirming that GCN2 indeed regulates BABA-induced stress. By contrast, *gcn2-1* seedlings were not impaired in BABA-IR against *H. arabidopsidis* CALA2, which is virulent on L*er* genotypes[43] (**Fig. 5b**). Hence, GCN2 does not regulate BABA-IR. Together, these results show that BABA-IR and BABA-induced growth reduction are controlled by separate signaling pathways.

DISCUSSION

Our study has shown that BABA-induced disease protection requires an intact *IBI1* gene (**Figs. 1**, **2b**, **3a** and **4b** and **Supplementary Figs. 1**, **2** and **3c**). In combination with our demonstration that only the active *R* enantiomer of BABA binds IBI1 *in planta* (**Fig. 3b** and **Supplementary Fig. 12**), our results provide plausible evidence that IBI1 is the plant receptor of BABA. Computational docking studies indicated that (*R*)-BABA binds the conserved L-Asp binding site of AspRS in a similar spatial orientation as L-Asp (**Supplementary Figs. 10** and **11**). The canonical L-Asp substrate of the enzyme is constantly processed and released as charged Asp-tRNA^{Asp}. Conversely, (*R*)-BABA cannot be aminoacylated and would eventually replace L-Asp from the binding pocket, thereby 'jamming' the protein's canonical AspRS activity. In support of this, BABA triggered enhanced aspartic acid accumulation in an enantiomer-specific manner (**Fig. 4b**) and stimulated GCN2-dependent eIF2α phosphorylation (**Fig. 4a**), which marks cellular accumulation of uncharged tRNA[40–42].

Our study raises one important question: why have plants evolved a receptor of a xenobiotic compound that is not produced by the plant? One possible explanation comes from our finding that *P. fluorescens* WCS417r bacteria failed to elicit ISR in *ibi1-1* plants (**Fig. 1c**). Considering the critical role of IBI1 in BABA perception, it is plausible that ISR-eliciting rhizobacteria produce BABA or a functional analog thereof. Indeed, *P. fluorescens* WCS417r-ISR and BABA-IR against *H. arabidopsidis* share similar signal transduction components and are both associated with priming of callose deposition[21]. It is also plausible that IBI1 contributes to basal disease resistance. Of the two *Arabidopsis* genes encoding nonplastid AspRS proteins, only *IBI1* showed increased transcription in response to *H. arabidopsidis* inoculation (**Fig. 2a**). Moreover, transgenic overexpression of *IBI1* increased basal resistance in the absence of BABA (**Fig. 2b** and **Supplementary Fig. 5**). In combination with selective uptake of aspartic acid by the pathogen, increased *IBI1* expression during pathogen infection would lead to more IBI1 protein that is deprived of AspRS activity. We propose that this denial of canonical activity, together with pathogen-induced translocation to the cytoplasm (**Fig. 2c** and **Supplementary Fig. 7**), triggers noncanonical defense activity by IBI1. (*R*)-BABA partially mimics this process by blocking the aspartic acid–binding pocket of IBI1, thereby depriving it from AspRS activity and priming its noncanonical defense response to pathogen attack.

Aminoacyl-tRNA synthetases are known for their ability to express noncanonical functions beyond translation, which have been attributed to their ability to interact with other proteins[44]. Interaction between IBI1 and (proteinaceous) cofactors could explain why purified IBI1:YFP lacks *in vitro* activity (**Supplementary Table 1** and **Supplementary Fig. 13**). Specific IBI1-protein interactions could also be responsible for the noncanonical defense activity of IBI1 in the cytoplasm (**Fig. 2c** and **Supplementary Fig. 7**). Human glutaminyl-tRNA synthetase exerts antiapoptotic activity through inhibitory interaction with the mitogen-activated protein triple kinase (MAPKKK) ASK1 (ref. 45). Therefore, it is tempting to speculate that IBI1 inhibits cytoplasm-localized plant MAPKKKs with repressive activity on plant immunity, such as MEKK1 and EDR1

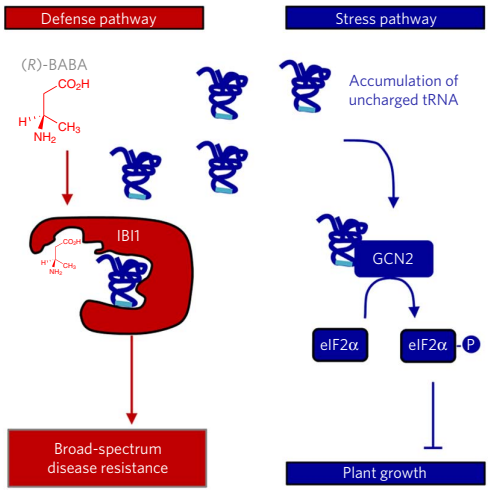

Figure 6 | The BABA receptor IBI1 controls BABA-IR and plant growth suppression via separate pathways. Binding of the *R* enantiomer of BABA to the L-Asp–binding site of IBI1 blocks canonical AspRS activity, which primes the protein for pathogen-inducible defense activity in the cytoplasm (red). Concurrently, the inhibitory activity of (*R*)-BABA on AspRS activity leads to accumulation of uncharged tRNAs, which triggers GCN2-dependent phosphorylation of the translation initiation factor eIF2α and suppression of plant growth (blue).

(refs. 46,47). Notably, amino acid alignments between IBI1 and the AspRS homolog At4g26870 revealed relatively high dissimilarity at the N terminus (**Supplementary Fig. 3a**). As At4g26870 does not regulate BABA-IR (**Supplementary Fig. 3c**), we propose that the noncanonical defense activity of IBI1 is determined by its unique N-terminal sequence. This hypothesis is in agreement with previous findings that noncanonical functions of aminoacyl-tRNA synthetases are determined by variable N- or C-terminal domains[44,48].

We conclude that plant perception of BABA is mediated by IBI1. The enzyme can switch from canonical AspRS activity to noncanonical defense activity upon pathogen infection. This response is strongly augmented by (*R*)-BABA, which blocks the L-Asp–binding site of the enzyme, thereby depriving the protein from AspRS activity and priming it for defense activity (**Fig. 6**). BABA-induced inhibition of AspRS activity also increases cellular accumulation of uncharged tRNA^{Asp}, which triggers GCN2-dependent eIF2α phosphorylation and stress-related growth repression independently from BABA-IR (**Fig. 6**). Hence, broad-spectrum disease protection by BABA can be uncoupled from the concurring plant stress response. Because BABA is perceived in a mechanistically similar manner by taxonomically unrelated plant species[31–33] (**Supplementary Fig. 8**), our discovery of the plant receptor of BABA opens new possibilities to protect crops against economically important crop diseases.

Received 11 June 2013; accepted 27 March 2014;
published online 28 April 2014

METHODS

Methods and any associated references are available in the online version of the paper.

References

1. Pieterse, C.M.J., Van der Does, D., Zamioudis, C., Leon-Reyes, A. & Van Wees, S.C.M. Hormonal modulation of plant immunity. *Annu. Rev. Cell Dev. Biol.* **28**, 489–521 (2012).
2. Conrath, U. *et al.* Priming: getting ready for battle. *Mol. Plant Microbe Interact.* **19**, 1062–1071 (2006).
3. Pastor, V., Luna, E., Mauch-Mani, B., Ton, J. & Flors, V. Primed plants do not forget. *Environ. Exp. Bot.* **94**, 46–56 (2013).

4. Kohler, A., Schwindling, S. & Conrath, U. Benzothiadiazole-induced priming for potentiated responses to pathogen infection, wounding, and infiltration of water into leaves requires the *NPR1/NIM1* gene in *Arabidopsis*. *Plant Physiol.* **128**, 1046–1056 (2002).
5. Jung, H.W., Tschaplinski, T.J., Wang, L., Glazebrook, J. & Greenberg, J.T. Priming in systemic plant immunity. *Science* **324**, 89–91 (2009).
6. van Hulten, M., Pelser, M., van Loon, L., Pieterse, C.M.J. & Ton, J. Costs and benefits of priming for defense in *Arabidopsis*. *Proc. Natl. Acad. Sci. USA* **103**, 5602–5607 (2006).
7. Walters, D. & Heil, M. Costs and trade-offs associated with induced resistance. *Physiol. Mol. Plant Pathol.* **71**, 3–17 (2007).
8. Ahmad, S., Gordon-Weeks, R., Pickett, J. & Ton, J. Natural variation in priming of basal resistance: from evolutionary origin to agricultural exploitation. *Mol. Plant Pathol.* **11**, 817–827 (2010).
9. Conrath, U. Molecular aspects of defence priming. *Trends Plant Sci.* **16**, 524–531 (2011).
10. Luna, E., Bruce, T.J.A., Roberts, M.R., Flors, V. & Ton, J. Next-generation systemic acquired resistance. *Plant Physiol.* **158**, 844–853 (2012).
11. Slaughter, A. *et al.* Descendants of primed *Arabidopsis* plants exhibit resistance to biotic stress. *Plant Physiol.* **158**, 835–843 (2012).
12. Beckers, G.J.M. & Conrath, U. Priming for stress resistance: from the lab to the field. *Curr. Opin. Plant Biol.* **10**, 425–431 (2007).
13. Gao, Q.M., Kachroo, A. & Kachroo, P. Chemical inducers of systemic immunity in plants. *J. Exp. Bot.* doi:10.1093/jxb/eru010 (2014).
14. Walters, D.R., Ratsep, J. & Havis, N.D. Controlling crop diseases using induced resistance: challenges for the future. *J. Exp. Bot.* **64**, 1263–1280 (2013).
15. Cohen, Y.R. β-aminobutyric acid–induced resistance against plant pathogens. *Plant Dis.* **86**, 448–457 (2002).
16. Zimmerli, L., Jakab, G., Métraux, J.-P. & Mauch-Mani, B. Potentiation of pathogen-specific defense mechanisms in *Arabidopsis* by β-aminobutyric acid. *Proc. Natl. Acad. Sci. USA* **97**, 12920–12925 (2000).
17. Ton, J. *et al.* Dissecting the β-aminobutyric acid–induced priming phenomenon in *Arabidopsis*. *Plant Cell* **17**, 987–999 (2005).
18. Singh, P. *et al.* The lectin receptor kinase-VI.2 is required for priming and positively regulates *Arabidopsis* pattern-triggered immunity. *Plant Cell* **24**, 1256–1270 (2012).
19. Návarová, H., Bernsdorff, F., Döring, A.-C. & Zeier, J. Pipecolic acid, an endogenous mediator of defense amplification and priming, is a critical regulator of inducible plant immunity **24**, 5123–5141 (2012).
20. Ton, J. & Mauch-Mani, B. β-amino-butyric acid–induced resistance against necrotrophic pathogens is based on ABA-dependent priming for callose. *Plant J.* **38**, 119–130 (2004).
21. Van der Ent, S. *et al.* Priming of plant innate immunity by rhizobacteria and β-aminobutyric acid: differences and similarities in regulation. *New Phytol.* **183**, 419–431 (2009).
22. Wu, C.-C., Singh, P., Chen, M.-C. & Zimmerli, L. L-Glutamine inhibits β-aminobutyric acid–induced stress resistance and priming in *Arabidopsis*. *J. Exp. Bot.* **61**, 995–1002 (2010).
23. Delaney, T.P. *et al.* A central role of salicylic acid in plant disease resistance. *Science* **266**, 1247–1250 (1994).
24. Flors, V. *et al.* Interplay between JA, SA and ABA signalling during basal and induced resistance against *Pseudomonas syringae* and *Alternaria brassicicola*. *Plant J.* **54**, 81–92 (2008).
25. Parker, J.E. *et al.* The *Arabidopsis* downy mildew resistance gene RPP5 shares similarity to the toll and interleukin-1 receptors with N and L6. *Plant Cell* **9**, 879–894 (1997).
26. Bell, C.J. & Ecker, J.R. Assignment of 30 microsatellite loci to the linkage map of *Arabidopsis*. *Genomics* **19**, 137–144 (1994).
27. Mauch-Mani, B. & Slusarenko, A.J. Production of salicylic acid precursors is a major function of phenylalanine ammonia-lyase in the resistance of *Arabidopsis* to *Peronospora parasitica*. *Plant Cell* **8**, 203–212 (1996).
28. Guo, M., Yang, X.L. & Schimmel, P. New functions of aminoacyl-tRNA synthetases beyond translation. *Nat. Rev. Mol. Cell Biol.* **11**, 668–674 (2010).
29. Nelson, B.K., Cai, X. & Nebenfuhr, A. A multicolored set of *in vivo* organelle markers for co-localization studies in *Arabidopsis* and other plants. *Plant J.* **51**, 1126–1136 (2007).
30. Duchêne, A.M. *et al.* Dual targeting is the rule for organellar aminoacyl-tRNA synthetases in *Arabidopsis thaliana*. *Proc. Natl. Acad. Sci. USA* **102**, 16484–16489 (2005).
31. Cohen, Y. 3-Aminobutyric acid induces systemic resistance against *Peronospore tabacina*. *Physiol. Mol. Plant Pathol.* **44**, 273–288 (1994).
32. Silué, D., Pajot, E. & Cohen, Y. Induction of resistance to downy mildew (*Peronospora parasitica*) in cauliflower by DL-β-amino-*n*-butanoic acid (BABA). *Plant Pathol.* **51**, 97–102 (2002).
33. Cohen, Y., Rubin, A.E. & Kilfin, G. Mechanisms of induced resistance in lettuce against *Bremia lactucae* by DL-β-amino-butyric acid (BABA). *Eur. J. Plant Pathol.* **126**, 553–573 (2010).
34. Cavarelli, J. *et al.* The active site of yeast aspartyl-tRNA synthetase: structural and functional aspects of the aminoacylation reaction. *EMBO J.* **13**, 327–337 (1994).
35. Schmitt, E. *et al.* Crystal structure of aspartyl-tRNA synthetase from *Pyrococcus kodakaraensis* KOD: archaeon specificity and catalytic mechanism of adenylate formation. *EMBO J.* **17**, 5227–5237 (1998).
36. Shrift, A., Bechard, D. & Harcup, C. Utilization of selenocysteine by a cysteinyl-tRNA synthetase from *Phaseolus aureus*. *Plant Physiol.* **58**, 248–252 (1976).
37. Ulmasov, B., Topin, A., Chen, Z., He, S.H. & Folk, W.R. Identity elements and aminoacylation of plant $tRNA^{Trp}$. *Nucleic Acids Res.* **26**, 5139–5141 (1998).
38. Lloyd, A.J., Thomann, H.U., Ibba, M. & Soll, D. A broadly applicable continuous spectrophotometric assay for measuring aminoacyl-tRNA synthetase activity. *Nucleic Acids Res.* **23**, 2886–2892 (1995).
39. Cestari, I. & Stuart, K. A spectrophotometric assay for quantitative measurement of aminoacyl-tRNA synthetase activity. *J. Biomol. Screen.* **18**, 490–497 (2013).
40. Dever, T.E. & Hinnebusch, A.G. GCN2 whets the appetite for amino acids. *Mol. Cell* **18**, 141–142 (2005).
41. Li, M.W., AuYeung, W.K. & Lam, H.M. The GCN2 homologue in *Arabidopsis thaliana* interacts with uncharged tRNA and uses *Arabidopsis* eIF2α molecules as direct substrates. *Plant Biol.* **15**, 13–18 (2013).
42. Zhang, Y. *et al.* GCN2-dependent phosphorylation of eukaryotic translation initiation factor-2α in *Arabidopsis*. *J. Exp. Bot.* **59**, 3131–3141 (2008).
43. Holub, E.B., Beynon, L.J. & Crute, I.R. Phenotypic and genotypic characterization of interactions between isolates of *Peronospora parasitica* and accessions of *Arabidopsis thaliana*. *Mol. Plant Microbe Interact.* **7**, 223–239 (1994).
44. Guo, M. & Schimmel, P. Essential nontranslational functions of tRNA synthetases. *Nat. Chem. Biol.* **9**, 145–153 (2013).
45. Ko, Y.-G. *et al.* Glutamine-dependent antiapoptotic interaction of human glutaminyl-tRNA synthetase with apoptosis signal-regulating kinase 1. *J. Biol. Chem.* **276**, 6030–6036 (2001).
46. Frye, C.A., Tang, D. & Innes, R.W. Negative regulation of defense responses in plants by a conserved MAPKK kinase. *Proc. Natl. Acad. Sci. USA* **98**, 373–378 (2001).
47. Kong, Q. *et al.* The MEKK1–MKK1/MKK2–MPK4 kinase cascade negatively regulates immunity mediated by a mitogen-activated protein kinase kinase kinase in *Arabidopsis*. *Plant Cell* **24**, 2225–2236 (2012).
48. Guo, M., Yang, X.L. & Schimmel, P. New functions of aminoacyl-tRNA synthetases beyond translation. *Nat. Rev. Mol. Cell Biol.* **11**, 668–674 (2010).

Acknowledgments

We thank S. van Wees, N. Halford, J. Lucas, J. Pickett, I. Feussner, X. Zhang, W. Kegge, D. Acoska, M. Roberts, V. Pastor, J. Gamir and B. Mauch-Mani for fruitful discussions, practical assistance and/or helpful feedback. *Arabidopsis* NahG B15 and L*er rpp5* seeds were kindly provided by J. Ryals (Research Triangle Park, USA) and J. Parker (Max Planck Institute, Cologne), respectively. The research was supported by a VENI grant to J.T. (no. 863.04.019) from the Netherlands Organisation of Scientific Research (NWO), a Biotechnology and Biological Sciences Research Council Institute Career Path Fellowship (no. BB/E023959/1) to J.T., a consolidator grant from the European Research Council (no. 309944-Prime-A-Plant) to J.T., a Research Leadership Award from the Leverhulme Trust (no. RL-2012-042) to J.T., European Union Seventh Framework Programme (FP7/2007-2013; n°265865-PURE) to J.T., a grant from the Felix Thornley Cobbold Agricultural Trust to J.T. and E.L. and a VICI grant (no. 865.04.002) to C.M.J.P. from NWO.

Author contributions

J.T. designed and supervised the research plan, performed experiments (mutant screen, map-based cloning, construction of transgenic lines, RT-qPCR and bioassays) and wrote the manuscript. E.L. performed experiments (map-based cloning, construction of transgenic lines, RT-qPCR, bioassays, confocal microscopy and IP assays), wrote the manuscript and provided intellectual input. M.v.H. performed experiments (mutant screen and bioassays) and provided intellectual input. Y.Z. performed experiments (map-based cloning and RT-qPCR) and provided intellectual input. O.B. performed experiments (GCN2 activity assays) and provided intellectual input. A.L. performed experiments (confocal microscopy and IP assays). P.P. performed experiments (MS). M.A.S. did computational modeling. B.C. did computational modeling and provided intellectual input. M.B. provided intellectual input. A.v.d.M. performed experiments (confocal microscopy). C.M.J.P. provided intellectual input. V.F. performed experiments (bioassays) and provided intellectual input.

Competing financial interests

The authors declare no competing financial interests.

Additional information

Supplementary information is available in the online version of the paper. Reprints and permissions information is available online at http://www.nature.com/reprints/index.html. Correspondence and requests for materials should be addressed to J.T.

ONLINE METHODS

Plant material and growth conditions. Genotypes of the *Arabidopsis* lines used are presented in **Supplementary Table 2**. Unless stated otherwise, seeds for plants in bioassays and gene expression experiments were planted in 60-ml pots containing a peat/sand mixture (2:1), stratified at 4 °C in darkness for 2 d and cultivated at 8.5 h light (150 µmol m^{-2} s^{-1}; 20 °C) and 15.5 h darkness (18 °C). For experiments with plants older than 3 weeks, 10-d-old seedlings were transplanted individually to 60-ml pots. To minimize environmental variation, plants for immunoblot analysis of eIF2α phosphorylation (western blots) were cultivated on half-strength MS agar (0.8%). *Solanum lycopersicum* (Micro-Tom) seeds were germinated in water for 5 d (darkness; 28 °C), transplanted to 100 ml-pots containing Scotts Levington M3 soil and cultivated at 16 h light (150 µmol m^{-2} s^{-1}; 26 °C) and 8 h darkness (21 °C).

Chemical treatments. Induction treatments with (*S*/*R*)-BABA (Sigma-Aldrich; A4420-7), (*R*)-BABA (Astatech 62363), (*S*)-BABA (Astatech; 62359), (±)-ABA (Sigma-Aldrich; A1049) or L-Asp (Sigma-Aldrich; A9256) were performed by injecting 10× concentrated 6-ml quantities into 60-ml pots once. Final soil concentrations are indicated in the figure legends of **Figure 1–5** and **Supplementary Figures 1–5**, **7–9**, **12** and **16**. Sodium-SA (Sigma-Aldrich; S3007) was applied by spraying a 0.5 mM solution onto 3-week-old plants. Unless stated otherwise, secondary elicitation treatments were performed 2 d after primary induction treatment. For *in planta* analysis of BABA-IBI1:YFP interaction, 5-week-old Col-0 wild-type and *ibi1-1 35S:IBI1:YFP-1* plants were treated twice with water, 1.2 mM (*R*)-BABA or 1.2 mM (*S*)-BABA 3 d apart. Five days after the second treatment, leaf material was harvested for protein extraction, IP and MS analysis. Agar-grown seedlings for western blot analysis (2-week-old) were sprayed once with 250 µM (*S*/*R*)-BABA to ensure synchronized activation of BABA-induced stress.

EMS mutagenesis, mutant screening and mapping. Approximately 10,000 Col-0 NahG seeds were EMS mutagenized as described[49]. Seeds from 20 to 30 M_1 plants per pot were pooled in M_2 families for screening. Of each M_2 family, 600 seedlings (~10 d old) were transplanted into 200-well trays (Teku; JP3050/230). Three-week-old plants were soil-drenched to a final concentration of 150 µM BABA. Two days later, plants were spray-inoculated with *H. arabidopsidis* (5×10^4 sporangiospores per ml) and maintained at 100% relative humidity. At 5–7 dpi, plants were evaluated for their phenotype, and sporulating plants were transplanted and rescued with 0.1 mg ml^{-1} Ridomil Gold (Syngenta). Loss of BABA-IR was confirmed in the M_3 generation, as described below. The screen identified 2 *ibi1* mutants (NahG *ibi1-1* and NahG *ibi1-2*), which were confirmed to be recessive and allelic on the basis of segregation analysis of F2 progeny from a backcross with NahG cross and a complementation cross, respectively. NahG *ibi1-1* was crossed with the L*er rpp5* mutant[25] to produce an F_2 mapping population, which was screened for *ibi* phenotypes. Initial mapping of *ibi1-1* was based on 30 susceptible F_2 plants using 22 SSLP markers[26]. Fine mapping was based on a selection of 621 of the most susceptible individuals from a total of 1,204 sporulating F2 plants isolated from the screen, using additional SSLP, CAPS and dCAPS markers, which were designed from polymorphisms between Col-0 and L*er* genomic sequences, using the TAIR Polymorphism/Allele search tool (http://www.arabidopsis.org/). Candidate genes in the fine-mapped region (*At4g31560-At4g32105*) were amplified from mutant cDNA by PCR using Phusion DNA polymerase (Finnzymes F-530S), sequenced and aligned to wild-type DNA using Vector NTI Advance 11 computer software (Invitrogen).

Selection for *ibi1* mutant genotypes in the Col-0 background. F2 progeny from a cross between NahG *ibi1-1* and Col-0 were analyzed by PCR using primers against *NahG*, wild-type *IBI1* and the mutant *ibi1-1* allele (**Supplementary Table 2**). Screening of 95 F2 plants revealed one heterozygous *ibi1-1*/*IBI1* recombinant without *NahG*, suggesting that *NahG* in line B15 is genetically linked to *IBI1*. PCR-based selection of selfed progeny provided the homozygous Col-0 *ibi1-1* mutant. Mutants *ibi1-3* and *ibi1-4* are derived from SALK (SALK-103893) and SAIL (SAIL-228-H03), respectively, and were selected for homozygous insertions using one T-DNA–specific primer and two gene-specific primers flanking the T-DNA insertions (**Supplementary Table 2**).

Resistance assays, stress assays and statistics. *H. arabidopsidis* strain WACO9 (compatible with Ws and Col genotypes) or CALA-2 (compatible with L*er*) were maintained on Ws NahG or L*er* plants, respectively. *H. arabidopsidis* assays were performed as described[21]. Plants (2- to 3-week-old) were inoculated with *H. arabidopsidis* (5×10^4 conidiospores per ml) at 2 d after chemical treatment. Unless stated otherwise, *H. arabidopsidis* colonization was determined microscopically at 7 dpi in Trypan blue–stained leaves, as described[10]. Differences in class distribution between treatments were analyzed for statistically significant differences by Fisher's exact tests (α = 0.05; SPSS, v19.0).

Callose depositions were examined at 2 dpi in Aniline blue- and calcofluor-stained leaves, using UV epifluorescence microscopy as described[17]. The effectiveness of callose was quantified by percentage of conidiospores, from which the proximal end of the emerging germ tube was encapsulated in callose. Statistical analyses were performed with average percentages per collected leaf (Student's *t*-test; α = 0.05; SPSS, v19.0). Additionally, the 'total number of callose-arrested spores'/'total number of nonarrested spores' ratios were tested for statistical significance against corresponding ratios from water-treated wild-type plants (binomial test; α = 0.05; SPSS, v19.0).

Assays to assess priming of *PR1* transcription were performed with 3-week-old plants. SA (0.5 mM) or *H. arabidopsidis* (5×10^4 conidiospores per ml) was sprayed onto shoots 2 d after root treatment with BABA (150 µM), and shoot samples were collected at different time points after SA application or 2 dpi with *H. arabidopsidis*. Statistical analysis was performed with normalized gene expression values (Student's *t*-test; α = 0.05; SPSS, v19.0).

P. cucumerina bioassays were performed as described[20]. Five-week old plants were soil-drenched with BABA or ABA and 2 d later were inoculated (2.5×10^6 spores per ml). Disease and colonization were evaluated microscopically at 7 dpi by assigning Trypan blue–stained leaves to different classes: (i) no cell death or fungal colonization; (ii) moderate necrosis at inoculation site but no pathogen colonization; (iii) full necrosis at the site of inoculation with restricted growth of fungal hyphae; and (iv) spreading necrosis and hyphal colonization beyond the sites of inoculation. Differences in class distribution between treatments were analyzed for statistically significant differences by Fisher's exact tests (α = 0.05; SPSS, v19.0).

Induced resistance assays with tomato and *B. cinerea* were performed largely as described[50]. Disease and colonization by *B. cinerea* were examined microscopically at 3 dpi in Trypan blue–stained leaves and assigned to different classes: (i) contained lesion and no hyphal growth outside the necrotic lesion; (ii) contained lesion with minimal hyphal growth beyond the lesion; and (iii) spreading lesion with extensive hyphal growth beyond the lesion. Differences in class distribution between treatments were analyzed for statistically significant differences by χ^2 or Fisher's exact tests (α = 0.05; SPSS, v19.0).

BABA-induced stress in young seedlings was recorded by digital photography at 10 d or 3 weeks after planting surface-sterilized seeds on control- and BABA-supplemented agar (500 µM BABA, half-MS; 0.8% agar). BABA-induced growth inhibition was determined in 2- to 3-week-old plants over a 7-d time interval after soil-drench treatment with BABA and is expressed as percentage fresh weight reduction compared to control-treated plants. Shapiro-Wilk tests for normality and a Levene's test for homogeneity of variances confirmed that these values meet the criteria for ANOVA. *Post hoc* analysis was performed using Fisher's least significant differences test (α = 0.05; SPSS, v19.0).

Generation of transgenic plants. Gateway cloning was used to produce an overexpression construct for a C-terminal IBI1:YFP fusion protein (**Fig. 2b**). The *IBI1* gene (1681 bp; without stop) was amplified by PCR from Col-0 cDNA (forward, 5′-CACCATGTCGTCGGAATCTGAAAT-3′, and reverse, 5′-GGGTGAAAGCCTTTGAGGGTCA)-3′) and cloned into pENTR (Invitrogen; 11791). A PCR-amplified fragment (m13/m13rev) from pENTR containing *IBI1* cDNA with boarding attL1 and attL2 sequences was used for recombination into pEarleyGate-101 (ref. 51). The binary plasmid was extracted (QIAprep Spin Miniprep Kit Cat. 27104) and sequenced (forward 1, 5′-CAATATGTGGTGACTTGCGA-3′; reverse 1, 5′-TCTCCATCTCCACAT CAAGA-3′; reverse 2, 5′-AAAGGATTCGCGACTCAGCT-3′) to confirm the correct insert. *Agrobacterium tumefaciens* GV3101 and *Arabidopsis ibi1-1* (Col-0) were transformed as described previously[52,53]. Selection of *Arabidopsis* transformants was performed by multiple spray applications of 120 mg l^{-1} glufosinate-ammonium PESTANAL (BASTA; Sigma; 45520). Selected T1 and T2 progenies were verified by PCR using *BAR*-specific primers (forward, 5′-GTCTGCACCATCGTCAAC-3′; reverse, 5′-GAAGTCCAGCTGCCAG AA-3′). Single insertion lines were selected on the basis of monogenic segregation of BASTA resistance in T2 progeny (3R/1S). Two independent homozygous overexpression lines were obtained and verified for enhanced

IBI1 transcription (**Supplementary Fig. 4a**), using RT-qPCR analysis with *IBI1*-specific primers (forward, 5′-GAGCGAGTGGTCATGCTTTTC-3′ and reverse, 5′-CGAGGGAAGAGGGATGTTTTC-3′).

Confocal laser scanning microscopy. YFP protein localization was analyzed in leaves of *ibi1-1 35S:IBI1-1* plants, using a Zeiss 780 Laser Scanning Microscope and Zen 2010 software. Leaves were placed on a slide with the upper epidermis facing the coverslip. YFP was excited with the 514-nm laser, and emission was collected from 525–600 nm. Chloroplast autofluorescence was excited with the 633-nm laser, and the emission was collected from 650–750 nm. Gain and offset were maintained at the same settings. Colocalization analysis of IBI1-YFP and ER marker protein was performed with an Inverted Zeiss LSM510-NLO microscope and a 40×/1.2 water immersion lens. Plants (*ibi1-1 35S:IBI1:YFP-1*) were crossed with ER-marker lines *ER-ck* or *ER-gk*[29] to obtain double transgenic F1 progenies: *ibi1-1 35:IBI1:YFP-1/ER-ck* and *ibi1-1 35S:IBI1:YFP-1/ER-gk*. Fluorescence spectra of CFP, GFP and YFP were collected from cotyledons of *ER-ck*, *ER-gk* and *ibi1-1 35S:IBI1:YFP* single transgenic lines, respectively. Fluorescent proteins (FPs) were excited with an argon 30-mW laser (458 nm, 488 nm and 514 nm) or with a Coherent Chameleon multi-photon laser. Emission spectra were collected from 478–500 nm for CFP, 480–520 nm for GFP and 525–600 nm for YFP. Epidermal peels from *ibi1-1 35S:IBI1:YFP-1/ER-gk* were obtained by removing the abaxial cell layer from fully expanded leaves. Fluorescence spectra of CFP, GFP and YFP in double transgenic F1 progenies were isolated, using previously recorded spectra from each FP-expressing single line, with the 'linear un-mixing' tool in LSM software (v4.2).

Protein binding assays, IP and immunoblotting. For *in planta* analysis of BABA-IBI1:YFP binding, proteins were extracted from 1 g pooled leaf material of water- and BABA-treated Col-0 and *ibi1-1 35S:IBI1:YFP-1*, using a standard protein extraction buffer (50 mM TRIS pH 7.5, 150 mM NaCl, 10% glycerol, 10 mM $MgCl_2$, 5 mM EDTA, 5 mM DTT, 0.6 mM PMSF and protease inhibitor cocktail (Sigma P9599)). Extracts were centrifuged twice for 15 min at 4 °C and 14,000g. Protein concentrations in the final supernatant (1 ml) were quantified using Bradford reagent (Sigma, B6916) and standardized to equal levels (2 mg ml^{-1}) before IP. Each IP was performed with 2 µg rabbit anti-YFP IgG antibody cross-linked to sepharose beads (Abcam; ab69314), following manufacturer's specifications, with slight modifications: before IP, sepharose beads were washed with 0.1% bovine serum albumin (BSA)-containing phosphate-buffered saline (PBS). After overnight IP on a rocking platform at 4 °C, beads were pelleted by centrifugation (3,000*g*, 1 min). Equal amounts of IBI1:YFP in IP pellets from *ibi1-1 35S:IBI1:YFP-1* plants were verified by YFP fluorescence. Proteins in pelleted sepharose beads were denatured by incubation for 5 min at 100 °C in 50 µl elution buffer (8 mM Tris, 4% SDS and 6 µl ml^{-1} of β-mercaptoethanol), after which the beads were pelleted by centrifugation (14,000*g*, 1 min) and the eluted supernatant was analyzed for BABA by MS, as detailed below.

For *in vitro* analysis of BABA-IBI1:YFP binding, BABA enantiomers were applied at three different stages of IBI1:YFP protein purification from *35S:IBI1:YFP-1* plants: crude protein extracts, Sephadex-purified protein extracts (PD-10 columns; Amersham Pharmacia Biotech, 281710) and immunoprecipitated IBI1:YFP protein. IBI1:YFP concentrations in all extracts were standardized on the basis of YFP fluorescence (ex.: A-485, em.: A-520; FLUOstar OPTIMA, BMG-ABTECH). Following application of 100 µM (*R*)-BABA or (*S*)-BABA, protein extracts were incubated at RT for 30 min on a rocking platform. IBI1:YFP in crude and Sephadex-purified extracts were immunoprecipitated as described above. Before protein denaturation in elution buffer, pellets were washed twice in protein extraction buffer (buffer details described above). Quantification of BABA in the eluted samples was performed by MS, as detailed below.

Protein extraction and immunoblotting for phosphorylation analysis of eIf2α was performed as described[54], using anti-phospho-eIF2α (Ser51) antibody (Cell Signaling Technology; 9721S), a polyclonal anti-TCTP antibody[54] and anti-rabbit IgG secondary antibody (Promega; S3731) in 1:1,000, 1:10,000 and 1:5,000 dilutions, respectively. Chemiluminescent detection was performed using the Western Star Immunodetection System (Applied Biosystems, Australia) and a VersaDoc MP 4000 CCD detector system with Quantity One software (Bio-Rad).

***In vitro* AspRS activity assays.** Purified IBI1:YFP protein was immunoprecipitated from protein extracts of overexpression plants (*ibi1-1 35S:IBI1:YFP-1*) using YFP-specific antibody (Abcam; ab69314) as described above. Activity assays were performed with immunoprecipitated IBI1:YFP in suspension with different reaction buffer components and conditions, as summarized in **Supplementary Table 1**. Aspartic acid (A9256), ATP (02055) and crude tRNA from wheat germ (R7876) were purchased from Sigma. $tRNA^{Asp}$ was synthesized through *in vitro* MEGAscript T7 transcription (Ambion, AM1333) of PCR products from *Arabidopsis* $tRNA^{Asp}$ genes (forward, 5′-TAATACGACTCACTATAGGGTCGTTGTAGTATAGTGGTAAG-3′, reverse, 5′-TGGCGCCGTTGCCGGGGATCG-3′). The $tRNA^{Asp}$ structure was given by incubating the $tRNA^{Asp}$ for 10 min. at 37 °C and subsequently maintained by the addition of $MgCl_2$ to a final concentration of 2 mM, as previously described[39]. AspRS activity was analyzed by a fluorometric pyrophosphate assay kit to detect the production of inorganic pyrophosphate, following the manufacturer's specifications (Abcam, ab112155) and using a plate reader (FLUOstar OPTIMA, BMG-ABTECH; ex.: A-340; em.: A-460). Pyrophosphate fluorescence in IBI1:YFP samples was compared to background fluorescence of immunoprecipitated samples from untransformed Col-0 lacking IBI1:YFP protein.

MS detection of aspartic acid and BABA. Solvents used for MS analyses were HPLC and/or MS grade: methanol (MeOH; Fluka; 34966), formic acid (HCOOH; Fluka; 06450), trifluoroacetic acid (TFA; Sigma-Aldrich; 302031) and water (H_2O; Waters; 232141B1). Amino acid extraction for aspartic acid quantification was performed from biologically replicated plant material ($n = 3$), as reported previously[55], with slight modifications: the lyophilized residues were resuspended into MeOH/H_2O/HCOOH (50:49.9:0.1) and vortexed for 2 min before MS analysis. Mass spectra of aspartic acid were obtained by MALDI-qTOF MS analysis, using a Synapt G2 mass spectrometer (Waters; Manchester; UK) in positive ionization mode ([M+H]; $m/z = 133.03$) and in 'target enhancement mass' function. MALDI was powered by a solid state laser emitting at 355 nm with a repetition rate of 2.5 kHz. The lock mass for MALDI-qTOF MS was sulfadimethoxine (Fluka; S1950000) and was acquired for 120 s, whereas samples were acquired for 180 s, using a spiral pattern with the laser firing conditions optimized at a plate speed of 50 Hz and attenuation level 140. Ion acquisition was performed at 10 kV with 11-kV hexapole bias and 7.0-V aperture. Mass ranges of scans (1 s) were defined from 50–1,200 Da. Matrix solution (α-cyano-4-hydroxycinnamic acid; CHCA; Sigma-Aldrich; C2020) was prepared at 5 mg ml^{-1} in MeOH/TFA (99.9:0.1). Each standard or sample was mixed with an equal volume of matrix solution (1:1) and spotted (2 µl) in triplicate onto 96-well stainless steel MALDI target plates (Waters). In parallel, sulfadimethoxine was prepared at 10 µg ml^{-1} in MeOH:H_2O (50:50; v/v) and spotted as lock mass for MALDI/TOF-MS analyses ([M+H]; $m/z = 311.08$). Droplets were allowed to dry, using a dry block heater (Dri-block DB3; Tecam; Italy) at 50 °C. Raw data were processed by Masslynx software (v4.1; Waters), and aspartic acid levels were quantified by extrapolating peak areas from a calibration curve and corrected for fresh weight. Stock solutions of aspartic acid (Sigma-Aldrich; A93100) were prepared in MeOH/H_2O/HCOOH (50:49.9:0.1; v/v) and used for calibration curves.

BABA was detected by both MALDI-qTOF MS and ESI-qTOF-MS (Zspray with NanoLockSpray; Waters), using a Synapt G2 mass spectrometer in positive ionization mode ([M+H] = 104.025) and in 'target enhancement mass' function. Samples from the IBI1:YFP pulldown assay (10 µl) were mixed with 10 µl of MeOH/H_2O/HCOOH (50:49.9:0.1; v/v). For MALDI-qTOF MS, the diluted extract was mixed with 20 µl CHCA matrix (5 mg ml^{-1}), and analyses were carried out as described above for aspartic acid. For ESI-qTOF-MS, source voltage at the injection capillary was set at 4 kV, the sampling cone was set at 20 kV and the extraction cone was set at 4 kV. Source and desolvation temperatures were set at 120 °C and 150 °C, respectively. Gas flows were adjusted at 20 l h^{-1} (cone gas), 0.5 Bar (nano-flow gas) and 600 l h^{-1} (purge and desolvation gas). Each sample was run out at 100 nl min^{-1} using a syringe pump (SP100iZ; WPI; UK), and data were acquired for 30 min. In parallel, leucine enkephalin ([M+H]; $m/z = 556.08$; Sigma-Aldrich; L9133) at 2 µg ml^{-1} in MeOH/H_2O (50:50; v/v;) was infused as lock mass. Standards of (*R*)-BABA and (*S*)-BABA (Astatech) were prepared in protein extraction buffer (see above) and diluted to appropriate concentrations with MeOH/H_2O/HCOOH (50:49.9:0.1; v/v) before analysis.

doi:10.1038/nchembio.1520

RNA extraction, reverse transcription and quantitative real-time PCR analysis. RNA extraction, cDNA synthesis and quantitative PCR reactions and data analysis were performed as described before[10,21]. After PCR amplification, melting curve analysis was performed to verify amplification of single PCR products. Relative transcript quantities were calculated according to $(1 + E)^{-\Delta Ct}$, where $\Delta C_t = C_t(\text{sample}) - C_t(\text{calibrator sample})$, and normalized to $(1 + E)^{-\Delta Ct}$ values of two reference genes, *At1g13440* and *At5g25760* (ref. 56).

Modeling of interactions between BABA enantiomers and Asp-RS proteins. BLAST of *Arabidopsis* IBI1 (UniProt: Q9M084) against the PDB identified protein crystal structures with a high sequence similarity. Two proteins from *P. pastoris* and *P. kodakaraensis* (PDB codes 1EOV and 3NEL, respectively) were selected on the basis of sequence similarity and availability of crystal structures. Sequence alignment was performed using the Protein Modeling protocol in Discovery Studio 3.5 (DS)[57]. Crystal structures were prepared for docking studies using the 'Prepare_Protein' tools, and binding sites were defined using the 'Define_and_Edit_Binding_Site' tool in DS. A 15-Å binding sphere was creased around previously identified binding residues of the crystal in 1EOV[40,41] and the co-crystallized aspartic acid coordinates in the crystal in 3NEL. Ligands (L-Asp, (*R*)-BABA and (*S*)-BABA) were prepared using the 'Prepare_Ligands' tool in DS for generating three-dimensional coordinates and pH-based ionization forms. Docking was performed using DS CDOCKER, which is a grid-based molecular docking method using CHARMm[58]. Random ligand conformations were generated from the initial ligand structure, using high temperature molecular dynamics at 1,000 K, followed by random rotations. Ligand confirmations were optimized using grid-based simulated annealing, followed by a final full force field minimization. Each docked ligand pose was assigned a score, which includes the internal force-field energy of the ligand, conformational entropy loss of the ligand, receptor-ligand hydrogen-bond interaction, solvation electrostatic energy change, hydrogen-bond donor/acceptor desolvation and hydrophobic energy. Comparisons were made between top-ranked ligand scores on the basis of generated three-dimensional interaction maps.

49. Kim, Y., Schumaker, K. & Zhu, J.-K. in *Arabidopsis Protocols* Vol. 323 (eds. Salinas, J. & Sanchez-Serrano, J.) 101–103 (Humana Press, 2006).
50. Audenaert, K., De Meyer, G.B. & Hofte, M.M. Abscisic acid determines basal susceptibility of tomato to Botrytis cinerea and suppresses salicylic acid–dependent signaling mechanisms. *Plant Physiol.* **128**, 491–501 (2002).
51. Earley, K.W. *et al.* Gateway-compatible vectors for plant functional genomics and proteomics. *Plant J.* **45**, 616–629 (2006).
52. Lin, J.J. Optimization of the transformation efficiency of *Agrobacterium tumefaciens* cells using electroporation. *Plant Sci.* **101**, 11–15 (1994).
53. Clough, S.J. & Bent, A.F. Floral dip: a simplified method for *Agrobacterium*-mediated transformation of *Arabidopsis thaliana*. *Plant J.* **16**, 735–743 (1998).
54. Berkowitz, O., Jost, R., Pollmann, S. & Masle, J. Characterization of TCTP, the translationally controlled tumor protein, from *Arabidopsis thaliana*. *Plant Cell* **20**, 3430–3447 (2008).
55. Pétriacq, P. *et al.* Inducible NAD overproduction in *Arabidopsis* alters metabolic pools and gene expression correlated with increased salicylate content and resistance to Pst-AvrRpm1. *Plant J.* **70**, 650–665 (2012).
56. Czechowski, T., Stitt, M., Altmann, T., Udvardi, M.K. & Scheible, W.R. Genome-wide identification and testing of superior reference genes for transcript normalization in *Arabidopsis*. *Plant Physiol.* **139**, 5–17 (2005).
57. Accelrys Software Inc., Discovery Studio Modeling Environment, Release 3.5 (San Diego, Accelrys Software Inc., 2012).
58. Wu, G., Robertson, D.H., Brooks, C.L. & Vieth, M. Detailed analysis of grid-based molecular docking: a case study of CDOCKER—A CHARMm-based MD docking algorithm. *J. Comput. Chem.* **24**, 1549–1562 (2003).